Decay of the High-K Isomeric State to a Rotational Band in 257Rf

Rissanen, J.; Clark, R. M.; Gregorich, K. E.; Gates, J. M.; Campbell, C. M.; Crawford, H. L.; Cromaz, M.; Esker, N. E.; Fallon, P.; Forsberg, Ulrika; Gothe, O.; Lee, I. -Y.; Liu, H. L.; Machiavelli, A. O.; Mudder, P.; Nitsche, H.; Pang, G.; Rice, A.; Rudolph, Dirk; Stoyer, M. A.; Wiens, A.; Xu, F. R.

Published in:
Physical Review C (Nuclear Physics)

DOI:
10.1103/PhysRevC.88.044313

2013

Decay of the high-K isomeric state to a rotational band in ^{257}Rf

J. Rissanen,[1,*] R. M. Clark,[1] K. E. Gregorich,[1] J. M. Gates,[1] C. M. Campbell,[1] H. L. Crawford,[1] M. Cromaz,[1] N. E. Esker,[1,2] P. Fallon,[1] U. Forsberg,[3] O. Gothe,[1,2] I.-Y. Lee,[1] H. L. Liu,[4] A. O. Machiavelli,[1] P. Mudder,[1,2] H. Nitsche,[1,2] G. Pang,[1] A. Rice,[1,2] D. Rudolph,[3] M. A. Stoyer,[5] A. Wiens,[1] and F. R. Xu[6]

[1]*Nuclear Science Division, Lawrence Berkeley National Laboratory, Berkeley, California 94720, USA*
[2]*Department of Chemistry, University of California, Berkeley, California 94720, USA*
[3]*Lund University, SE-221 00 Lund, Sweden*
[4]*Department of Applied Physics, Xi'an Jiaotong University, Xi'an 710049, China*
[5]*Lawrence Livermore National Laboratory, Livermore, California 94550, USA*
[6]*School of Physics, Peking University, Beijing 100871, China*

(Received 15 August 2013; published 11 October 2013)

The ^{257}Rf isotope has been populated via the ^{208}Pb(^{50}Ti, n) fusion-evaporation reaction and delayed γ-ray and electron decay spectroscopy has been performed. The existence of a high-K isomeric state in ^{257}Rf has been confirmed. The isomeric state decays into a rotational band based on the $11/2^-[725]$ excitation, which was observed up to spin of $(23/2^-)$. Three multipolarity-$E1$ γ transitions depopulating the isomeric state have been observed, which fixes the spin for that state to $(21/2^+)$. This assignment agrees with theoretical predictions calculated with the microscopic-macroscopic approach, which suggest the isomeric state to be formed by coupling an unpaired $11/2^-[725]$ quasineutron to the $(1/2^-[521] \otimes 9/2^+[624])_{5^-}$ two-quasiproton state. The same two-quasiproton excitation is possible for the lowest isomer in ^{256}Rf.

DOI: 10.1103/PhysRevC.88.044313 PACS number(s): 23.20.Lv, 23.35.+g, 27.90.+b

I. INTRODUCTION

According to the liquid drop model, nuclei with $Z \geqslant 104$ would immediately fission as a result of the massive Coulomb repulsion between protons [1]. However, elements do exist beyond that limit, and they are called "superheavy elements." These nuclei are relatively stable due to a variety of effects, including nuclear deformation, nuclear pairing, and quantum-mechanical shell effects. The notion of shell stabilization leads to the prediction of an "island of stability," where the nuclei are relatively long-lived with magic numbers of protons or neutrons. There exist different theoretical predictions for these magic numbers, for example, $Z = 114$, $N = 184$ [2], $Z = 124$, $N = 184$ [3], and $Z = 120$, $N = 172$ [4], although the extent and magnitude of these shell effects remain to be determined experimentally.

One way to investigate properties of the superheavy elements is to perform detailed spectroscopic studies of nuclei near the $Z = 100$ and $N = 152$ deformed shells. By using this approach, one can identify the active Nilsson states near the Fermi surface. Of specific interest are the so-called K isomers. Unpaired nucleons in axially symmetric nuclei couple their angular momenta to states with total spin projection K onto the symmetry axis. The K-quantum-number values can be large, in which case the γ-ray transitions from high-K into low-K states are strongly hindered, leading to formation of relatively long-lived isomeric states. This kind of isomer has been observed in several isotopes in the region; see, for example, Refs. [5–19]. By identifying high-K multiquasiparticle (QP) isomers and studying their decays to states with lower K, one can learn about single-particle energies, pairing correlations, and excitation modes in the heaviest nuclei.

^{257}Rf ($Z = 104$, $N = 153$) has two α-decaying states: a ground state based on the $1/2^+[620]$ configuration (^{257}Rf^{g}) and a high-spin isomeric state (^{257}Rf^{m1}) based on the $11/2^-[725]$ excitation at $\approx$70 keV [13,20,21]. In addition, a second isomeric state at around 1 MeV (^{257}Rf^{m2}) has recently been observed [12,13,16]. The decay of this higher-lying isomer is of particular interest, since it can be formed by the coupling of an odd neutron to a two-QP excitation in the ^{256}Rf core. Therefore, by studying the isomer decay in ^{257}Rf, it is possible to gain information about the structure of the core nucleus. The higher-lying isomer (^{257}Rf^{m2}) has been suggested to decay through a rotational band based on the $11/2^-$ isomeric state (^{257}Rf^{m1}), although that band has not been seen in earlier studies [13,16]. In this paper, the decay of that 3-QP isomer to experimentally observed rotational levels is reported. In addition to the isomer decay itself, the results of this work are important since the ^{257}Rf nucleus is the heaviest nucleus for which a rotational band has been observed so far.

II. EXPERIMENTAL

The ^{257}Rf nuclei were produced via the ^{208}Pb(^{50}Ti, n) fusion-evaporation reaction in an experiment using the Berkeley gas-filled Separator (BGS) [22] at the 88-Inch Cyclotron of the Lawrence Berkeley National Laboratory (LBNL). Two different targets and beam energies were used in the experiment. The first target (labeled as I) comprised a stack of two Pb foils evaporated on $\approx$35 μg/cm^2 thick carbon backings, the target foils facing toward an additional $\approx$40 μg/cm^2 thick carbon foil between the Pb layers. The second target (II) had only one Pb layer consisting of four Pb foils evaporated on Ti backings, positioned on a target wheel such that the beam was incident on the Ti first. Three of the Ti backings had a thickness of $\approx$1.4 mg/cm^2 (IIa) and one $\approx$0.9 mg/cm^2 (IIb).

*juhorissanen@lbl.gov

TABLE I. Different target and beam energy combinations used in this work. The beam energy E_{Beam} is given in the laboratory frame and the E^* is the center-of-target excitation energy.

Target	Hours on target	E_{Beam} (MeV)	E^* (MeV)
I	124	238	19
I	16	243	23
II(a)	83	258	19
II(b)			26

When prepared, the Pb foils in both target sets had a thickness of ≈400 μg/cm^2, which may have been somewhat decreased due to previous use. The target sets were mounted on the perimeters of two separate rotating target wheels. The beam energies were optimized using the excitation energy function of Ref. [23], and the energy loss in the target and the backing was calculated using the SRIM code [24]. The target and beam energy combinations are presented in Table I.

A new differential pumping system was used to separate the 0.5-Torr He gas inside the BGS from the beamline vacuum. Evaporation residues were separated from the beam and other reaction products in the BGS according to their magnetic rigidities and passed through a multiwire proportional counter (MWPC) before being implanted in the upgraded BGS focal plane (FP) detector.

The FP detector consists of three 64-mm × 64-mm, 1-mm-thick double-sided silicon strip detectors (DSSSDs), having 32 strips on each side. The strips on the back side were electrically connected in groups of three, which combined with the front side strips give a total of 128 channels. The DSSSDs were positioned to form three sides of the corner of a cube, so that the relative angle between individual detectors was 90 deg. An additional hexagonal-tunnel detector, located upstream to the beam and consisting of six Single-sided silicon detectors (SSSDs) shaped to fit against the focal plane, was also used. The four additional strips per SSSD detector give total number of 24 extra electronics channels. The FP detector (DSSSDs only) has a simulated detection efficiency of 70% for α particles, which increases up to 85% when combined with the upstream SSSDs.

The FP DSSSD configuration was designed to accommodate three clover Ge detectors [25] to measure γ radiation. Each clover was placed directly behind one side of the corner cube DSSSD configuration, behind the 2-mm-thick Al backplate of the focal plane, at ∼4 mm from the DSSSDs. Source measurements using standard γ-ray sources for the energy and efficiency calibrations of the detectors resulted in an absolute photopeak efficiency for the clover detectors of 32.1(5)% at 122 keV. However, two of the crystals were removed from the analysis due to bad performance, which decreased the efficiency to 25.1(5)%.

III. RESULTS

Potential Rf implantation events were identified by either a signal in the MWPC detector or a time-of-flight (TOF) signal between the MWPC and DSSSD, in coincidence with an implant in a DSSSD pixel (7.0 MeV < E_{DSSSD} < 17.0 MeV). In addition to the ^{257}Rf isotopes, some ^{256}Rf residues were produced via the ^{208}Pb(^{50}Ti, $2n$) reaction. These isotopes were distinguished by comparing their ground-state decay properties: ^{256}Rf has a very high fission branch (≈100%) whereas ^{257}Rf has a strong α branch (≈80%) [21]. The Rf isomer decays were identified by searching for a delayed conversion electron (E_e = 50–2000 keV, Δt = 15–1200 μs) signal within the same pixel of the DSSSD that registered the implanted recoil [26].

TABLE II. The observed numbers of r-e, r-e-α, r-α, r-f, and r-e-f events for different beam and target combinations.

Target	E_{Beam} (MeV)	Σ(r-e)	Σ(r-e-α)	Σ(r-α)	Σ(r-e-f)	Σ(r-f)
I	238	1113	479	3949	94	1463
I	243	33	14	91	9	100
II	258	513	93	641	209	2026

A total of 1659 recoil-electron (r-e) events were observed during the experiment. Of those events, 586 could be unequivocally associated with ^{257}Rf residues with the charasteristic α decay (r-e-α) with E_α = 8.32–9.2 MeV. In addition, 312 recoil-electron-fission (r-e-f) events and 19 recoil-electron-electron-fission (r-e-e-f) events were observed, which were mainly associated with ^{256}Rf. The observed events corresponding to the different beam and target combinations are presented in Table II and the electron energy spectra from r-e-f and r-e-α events are shown in Fig. 1. Due to pile-up summing of the recoil implantation and conversion energy signals in the FP detector, an additional time-dependent correction has been implemented to electron energies.

The γ-ray spectrum obtained in prompt coincidence with the electron bursts for all r-e events that did not have a spontaneous fission event following the electron (shown in Fig. 2) was used to determine the energies and relative intensities of the γ transitions related to the ^{257}Rf^{m2} isomer decay, presented in Table III. Since the detection efficiency for fission events is close to 100%, this yields a clean ^{257}Rf spectrum with better statistics compared to r-e-α events. For comparison, the γ rays in coincidence with the electrons from the decays of ^{256}Rf (r-e-f) are shown in Fig. 3. The 900-keV transition in Fig. 3 associated with ^{256}Rf events is known from

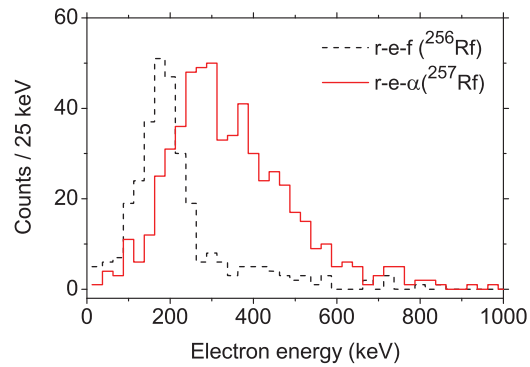

FIG. 1. (Color online) Electron energy spectrum from r-e-α (^{257}Rf) and r-e-f (^{256}Rf) events.

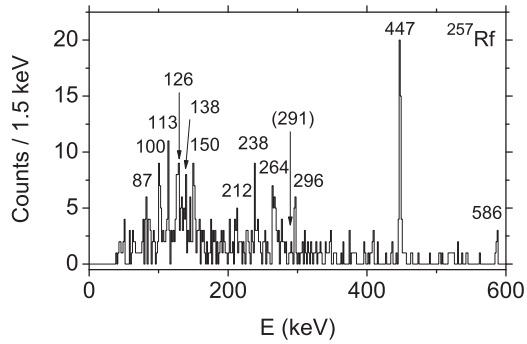

FIG. 2. Energy spectrum of γ rays in coincidence with the recoil electrons, which did not have a spontaneous fission event following the electron.

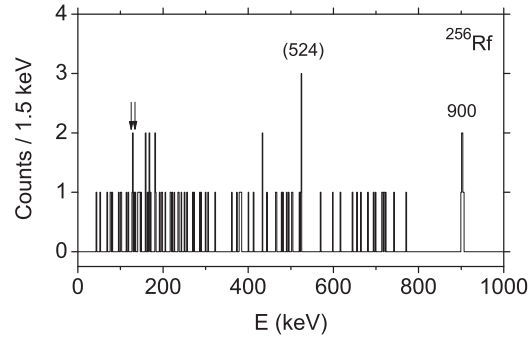

FIG. 3. Energy spectra of γ rays in coincidence with the recoil electrons, which had a spontaneous fission event following the electron (r-e-f). The arrows show the locations of the most intense Rf x-ray peaks.

previous work [12], whereas the tentative 524-keV transition has not been previously observed. However, with the low statistics, it could not be confirmed as a peak nor could it be placed in the level scheme of ^{256}Rf.

The γ energies and the related uncertainties have been determined by performing a standard Gaussian fit to each peak but using multiple spectra, which were achieved with different conditions (different gates, bin widths, addback or no addback) and the average energy value has been adopted. The maximum deviation of the fitted energies for each γ line has been taken as an extra uncertainty, to which the uncertainties of the energy calibration and the fit centroids have been added quadratically. The proposed decay scheme of the higher-lying isomeric state, shown in Fig. 4, has been constructed based on these γ energies and the related intensities, which were measured by treating the four crystals of each clover as individual detectors (no addback). The spin assignments shown in the scheme are discussed in more detail in Sec. IV A1.

TABLE III. γ rays following the decay of the high-K isomeric state observed in this work. Intensities are corrected with the detector efficiency and normalized to the intensity of the 446.8-keV transition. The intensities of the 125.4-keV and 149.9-keV transitions have been corrected for Rutherfordium $K_{\alpha 2}$ and $K_{\beta 1,3}$ x-ray intensities, respectively. The notation ^{X} stands for Rutherfordium $K_{\alpha 1}$ x ray.

E_γ(keV)	I_γ	$I_i^\pi \rightarrow I_f^\pi$	Multipolarity
86.9(14)	11(5)	$(13/2^-) \rightarrow 11/2^-$	$M1$
100.4(6)	14(5)	$(15/2^-) \rightarrow (13/2^-)$	$M1$
113.1(5)	11(5)	$(17/2^-) \rightarrow (15/2^-)$	$M1$
125.4(9)	7(4)	$(19/2^-) \rightarrow (17/2^-)$	$M1$
133.4(5)^{X}	5(4)		
138.4(7)	8(4)	$(21/2^-) \rightarrow (19/2^-)$	$M1$
149.9(7)	4(3)	$(23/2^-) \rightarrow (21/2^-)$	$M1$
212.2(7)	7(4)	$(17/2^-) \rightarrow (13/2^-)$	$E2$
238.3(9)	10(5)	$(19/2^-) \rightarrow (15/2^-)$	$E2$
263.9(10)	12(6)	$(21/2^-) \rightarrow (17/2^-)$	$E2$
(291)		$(23/2^-) \rightarrow (19/2^-)$	$(E2)$
295.6(7)	19(7)	$(21/2^+) \rightarrow (23/2^-)$	$E1$
446.8(7)	100(20)	$(21/2^+) \rightarrow (21/2^-)$	$E1$
586.1(13)	24(11)	$(21/2^+) \rightarrow (19/2^-)$	$E1$

The approximate de-excitation energy of the high-lying isomeric state ^{257}Rf^{m2} can be determined by adding the γ-ray energy to the energy of the conversion electron burst on an event-by-event basis. The obtained total excitation energy curve is presented in Fig. 5. The maximum energy extracted from the curve ($E \approx 1035$ keV) agrees with the value ($E \approx 1050$ keV) reported in Ref. [16] and is close to the energy difference between the isomeric states in ^{257}Rf, $E = 1011.2(4)$ keV determined from experimental γ energies (see Fig. 4), providing further support to the proposed decay scheme. The energy resolution of the DSSSDs for conversion electrons has been estimated to be ≈30 keV.

The time difference between the recoil implants and the subsequent electron bursts for all r-e-α events (^{257}Rf) is shown

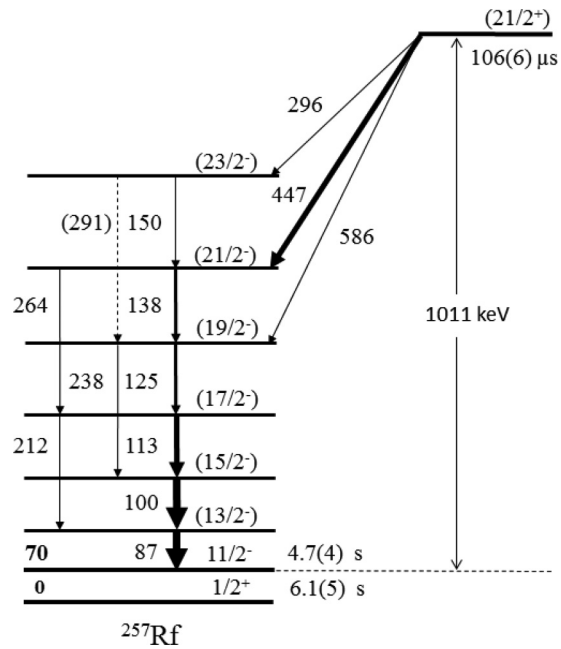

FIG. 4. Decay scheme of the high-K isomeric state in ^{257}Rf. The energies are in kilo electron volts and the arrow widths correspond approximately to the transition intensities. The energy of the $11/2^-$ state could not been determined in this work and has been taken from Ref. [21].

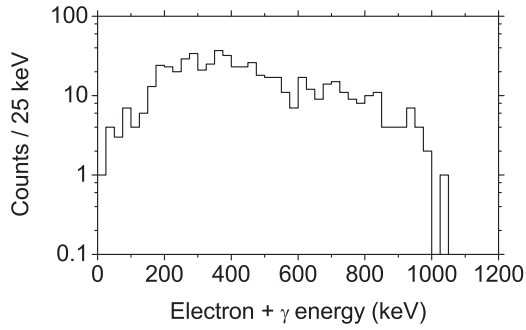

FIG. 5. Energy spectrum of conversion electron bursts from r-e-α events added to the energy of coincident γ rays on an event-by-event basis.

in Fig. 6. The half-life of the high-lying isomer ^{257}Rf^{m2} was obtained by fitting a single-component exponential decay with statistical weighting to the time spectra. The resulting half-life value $t_{1/2} = 106 \pm 6\mu$s does not agree with the earlier $134.9 \pm 7.7\mu$s [16] or $t_{1/2} = 160^{+42}_{-31}\mu$s [13]. However, it is in agreement with the value $t_{1/2} = 109 \pm 13\mu$s mentioned in Ref. [12]. We reanalyzed the data of Ref. [16] and found that the earlier fit had not properly accounted for the dead time of the acquisition system. Taking this into account yields a value $t_{1/2} = 110 \pm 5\mu$s, which is consistent with the present result.

In addition, our other half-life values obtained in this work for ^{257}Rf^{m1}, ^{257}Rf^{g}, and ^{256}Rf^{g} are in good agreement with the literature values, as shown in Table IV. The half-life of the $1/2^+$ ground state (^{257}Rf^{g}) was determined from r-α-α events as a time difference between the recoil implant and the first-generation α particle with E_α(^{257}Rf decay) = 8.4–8.85 MeV and E_α(^{253}No decay) = 7.9–8.2 MeV. The second-generation α-particle requirement was needed to remove the ^{257}Lr α events following the electron capture decay of ^{257}Rf [13]. In this case a small constant background component was added to the single-component exponential decay fit. The half-life of the $11/2^-$-isomeric state (^{257}Rf^{m1}) was determined from r-e-α events as a time difference between the electron burst and the α particle with $E_\alpha = 8.85$–9.2 MeV. The α energy spectrum used to determine the corresponding α gates is shown in Fig. 7. The half-life of the ^{256}Rf ground state was obtained

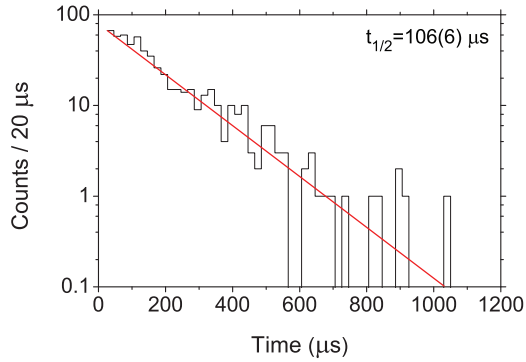

FIG. 6. (Color online) Electron decay curve for all r-e-α events. The thick red (gray) line is the fitted exponential decay curve.

TABLE IV. Half-life values determined in this work compared to the values found in literature. See text for more details.

Nuclide	$t_{1/2}$ (this work)	$t_{1/2}$ (literature)
^{257}Rf^{m2}	106 ± 6 μs	109 ± 13 μs [12]
^{257}Rf^{m1}	4.7 ± 0.4 s	4.6 ± 0.3 s [16]
^{257}Rf^{g}	6.1 ± 0.5 s	5.5 ± 0.4 s [21]
^{256}Rf	6.9 ± 0.2 ms	6.67 ± 0.09 ms [12]

from the time difference between the recoil implant and the subsequent fission event (r-f).

IV. DISCUSSION

A. Properties of the rotational band based on the lower isomeric state in ^{257}Rf

The existence of two α-decaying states in ^{257}Rf has been known for some time [20]. α decays of these states can be distinguished based on different α energies. The observed r-e-α events are clearly correlated with the α lines originating from the isomeric state, as already shown in Fig. 2 of Ref. [16]. These α lines have not been seen in the decay of ^{257}Rf atoms produced by ^{261}Sg α decay instead of directly created in a fusion evaporation [21]. The ^{261}Sg isotope has a low spin ($3/2^+$ [21]) and populates only the low-spin states in ^{257}Rf. Therefore, we assume that the γ lines shown in Fig. 2 lie above the $(11/2^-)$ isomeric state.

The spin of the low-lying isomer $(11/2^-)$ has been derived from its α-decay properties in Ref. [13]. A rotational band based on the $11/2^-$ isomeric state populated by the decay of a higher-lying isomeric state has been suggested in earlier studies [13,16]. However, this interpretation has not been based on solid experimental evidence. Only two γ transitions at 447 and 586 keV were observed in Ref. [16] and they were interpreted to directly depopulate the higher-lying isomeric state. The decay scenario proposed in that reference was based on the rotational-model estimates for the level energies and the sum energy plot of the conversion electrons and the

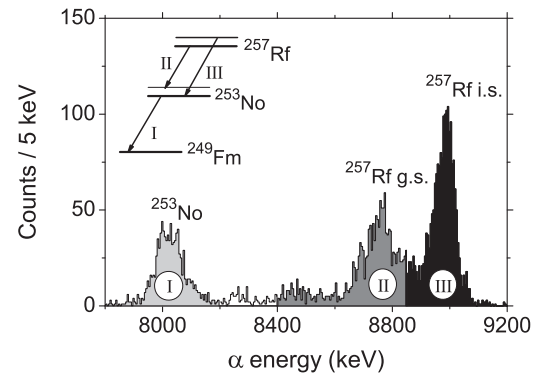

FIG. 7. α energy spectrum from r-α events with an inset showing a simplified α-decay scheme of the ground state and the first isomeric state in ^{257}Rf. The colored areas correspond to different α gates: ^{253}No decay (light gray), ^{257}Rf ground-state decay (dark gray), and ^{257}Rf isomeric state decay (black).

coincident γ lines. With the higher-statistics data in this work, the properties of the high-K isomeric state and its decay into a rotational band could be confirmed, as shown in following subsections.

1. Spin assignments

Tentative 73- and 159-keV transitions, proposed as the lowest $M1$ and $E2$ transitions of a rotational band, were suggested in Ref. [16], but were not observed in this work. Instead, the lowest observed transition in the band has an energy of 87 keV and it is assumed to connect to the band head. We have studied the validity of that assumption based on observed level energies, which, for a rotational band in an axially deformed nucleus with total spin projection K onto the symmetry axis, can be expressed by a simple rotational-model formula:

$$E = E_0 + \frac{\hbar^2}{2J}[I(I+1) - K^2], \tilde{} \qquad (1)$$

where E_0 is the band-head energy, J is the moment of inertia, and I is the spin of the rotational state. We have used the spin-fitting method analogous to Refs. [27,28] to fit the experimental level energies of the rotational band for different band-head spins I_0 with two fitting parameters E_0 and $\hbar^2/2J$ assuming the 87-keV transition as the lowest transition. When a correct I_0 is assigned, the calculated energies coincide with the observed result well. If I_0 is shifted away from the correct value, the root mean square error (RMSE) of the fit will increase drastically. This is illustrated in Fig. 8(a), where the RMSEs of fits with different I_0's are plotted. A clear minimum at $I_0 = 11/2$ can be observed, suggesting the 87-keV transition as the $13/2^- \rightarrow 11/2^-$ transition and the low-lying isomeric state as the band head, which agrees with the α decay data [13].

To verify the position of the 87-keV transition as the lowest transition, we have kept $I_0 = 11/2$ and compared the fitting results for different possibilities for the lowest $M1$ transition: (i) the 73-keV transition, (ii) the 87-keV transition, and (iii) the 100-keV transition, respectively. The fits were performed for the four lowest $M1$ transitions for each case. The resulting RMSE values plotted in Fig. 8(b) clearly favor option (ii). In addition, the rotational parameter $\hbar^2/2J = 6.6$ was fit for the rotational band without the 73-keV transition and $\hbar^2/2J = 5.9$ with that transition, respectively. The former value is consistent with the values determined from experimental level energies for the ^{256}Rf core (6.8) and other known $N = 153$ isotones, 6.6 for the $7/2^+$ band in ^{251}Cf and 6.7 for the $7/2^+$ band in ^{249}Cm. Based on these arguments, the tentative 73-keV and 159-keV transitions of Ref. [16] were not considered further in our level scheme.

2. Gyromagnetic ratios

As shown in Fig. 4, we interpret the γ-ray spectrum as arising from the decay of a strongly coupled rotational band, with strong $M1$ and weaker $E2$ transitions, based on the $11/2^-$ isomeric state. The intrinsic gyromagnetic ratios g_K for the rotational states were calculated from the

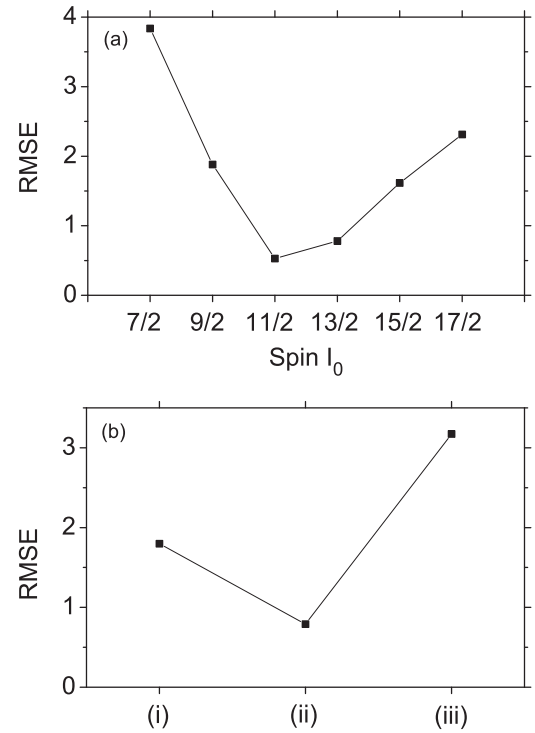

FIG. 8. The RMSE deviations for (a) various band-head spin assignments and (b) different possibilities as the lowest $M1$ transition. The options in the lower figure (b) correspond to (i) 73-keV transition, (ii) 87-keV transition, and (iii) 100-keV transition. See text for more details.

experimentally determined intraband $M1/E2$ branching ratios of the depopulating transitions and level energies for given K quantum number using rotational model expressions [29]:

$$\frac{g_K - g_R}{Q_0} = 0.933\frac{E_1}{\delta\sqrt{I^2-1}}, \qquad (2)$$

where δ is the quadrupole/dipole mixing ratio, calculated from

$$\frac{\delta^2}{1+\delta^2} = \frac{2K^2(2I-1)}{(I+1)(I-1+K)(I-1-K)}\frac{E_1^5}{E_2^5}\frac{I_2^\gamma}{I_1^\gamma}. \qquad (3)$$

Here E and I^γ refer to experimental γ energies (in million electron volts) and intensities and the subscripts 1,2 refer to $\Delta I = 1, 2$ transitions, respectively. The rotational g factor is taken as $g_R \approx Z/A$ and $Q_0 = 14.3\,eb$ is the intrinsic quadrupole moment assuming a quadrupole deformation of $\beta_2 = 0.256$, which was calculated for ^{256}Rf by using equation $\beta^2 \approx 1224/[E(2_1^+)A^{7/3}]$ [30] and $E(2_1^+) = 44.8$ keV [31]. Equation (2) assumes a well-defined K value and yields only the magnitude of δ, not its sign. Individual δ^2 and $|(g_K - g_R)/Q_0|$ values for the rotational levels have been tabulated in Table V, calculated using the γ energies and intensities from Table III.

The gyromagnetic factor g_K should be constant for all rotational states within the same band and is often used to distinguish between different configurations. The weighted average of all the rotational states, $|(g_K - g_R)/Q_0| = 0.034(7)$, was determined assuming $K = 11/2$. It can be compared to the theoretical values calculated from the asymptotic Nilsson

TABLE V. $g_K - g_R/Q_0$ ratios for the levels in the $K^\pi = 11/2^-$ rotational band.

Spin ($\hbar$)	δ^2	$(g_K - g_R)/Q_0$
17/2	0.12(8)	0.035(12)
19/2	0.15(11)	0.032(12)
21/2	0.13(8)	0.035(11)
	Average	0.034(7)

quantum numbers using the relation

$$Kg_K = \sum g_\Omega = \sum \Omega\left[g_\lambda + (g_\Sigma - g_\lambda)\frac{\langle s_3\rangle}{\Omega}\right], \qquad (4)$$

where Ω, λ, and Σ are the projections of the total, orbital, and intrinsic angular momenta of the nucleon onto the symmetry axis, respectively, with $g_\lambda = 0$ and $g_\Sigma = -3.83$ for neutron configurations. Those values were attenuated by the commonly used factor 0.6 [29]. The expectation value of the intrinsic spin, $\langle s_3\rangle$ was taken from Ref. [32]. The lowest single-particle excitations in the $N = 153$ isotopes are $1/2^+[620]$, $3/2^+[622]$, $7/2^+[613]$, and $11/2^-[725]$ [13]. Of those excitations, the calculated value for the $11/2^-[725]$ configuration, $(g_K - g_R)/Q_0 = 0.040$, is in agreement with the experimental value. A theoretical value for the $7/2^+[613]$ excitation is also close, as shown in Fig. 9. The $1/2^+[620]$ and $3/2^+[622]$ excitations are out of the range of Fig. 9 and can be clearly ruled out. The consistency of experimental values for different levels, as well as the good agreement between the experimental and theoretical values, give strong support for the $11/2^-[725]$ excitation.

B. Structure of the higher-lying isomeric state in ^{257}Rf

The spin and parity of the ^{257}Rf^{m2} isomer can be derived from the multipolarities of the transitions directly depopulating that state. The observation of three transitions with energies of 295.6, 446.8, and 586.1 keV populating three consecutive states in the rotational band requires that the middle transition, with $E = 446.8$ keV, has $L = 1$. The case of multipolarity $L = 2$ means that either the 295.6-keV or 586.1-keV transition would have $L > 2$, which is very unlikely. Therefore, the most likely scenario is that we are seeing three $L = 1$ dipole transitions depopulating the isomer. We can determine the electromagnetic character of these dipole transitions by considering the x-ray yield associated with internal conversion of the transitions. If the three transitions were of $M1$ type, they would be strongly converted, yielding a total of ≈60 $K_{\alpha 1}$ x-ray transitions. If the 446.8-keV transition was $M1$ and either the 295.6-keV or 586.1-keV transition were $E2$, the total $K_{\alpha 1}$ x-ray yield would be 40 and 55, respectively. An $E1$ multipolarity for the three transitions yields a total intensity of ∼3 $K_{\alpha 1}$ x rays, which is in good agreement with the observed intensity 5(4) of the Rutherfordium $K_{\alpha 1}$ line peak at 133.4 keV. Therefore, one can conclude that the three transitions decaying from the 3-QP isomer are likely $E1$s, implying that the isomeric state has $K^\pi = (21/2^+)$.

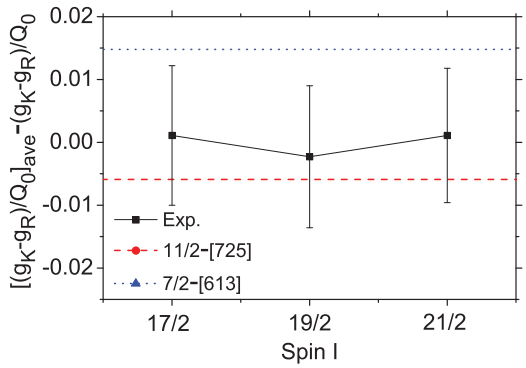

FIG. 9. (Color online) Experimentally determined $(g_K - g_R)/Q_0$ ratios, presented as differences from the average value $[(g_K - g_R)/Q_0]_{\rm ave} = 0.034(7)$, compared with theoretical estimates for two different neutron configurations.

This assignment is in agreement with the calculated hindrance factors for the depopulating transitions. For axially deformed nuclei, transitions with large ΔK are strongly hindered, causing isomerism. The half-lives of the resulting K isomers depend on the differences in transition energies depopulating the isomers and on the K forbiddenness, which is quantified by the factor

$$f_\nu = [(t_{1/2})\text{exp}/(t_{1/2})_{\rm WU}]^{1/\nu}. \qquad (5)$$

Here, $(t_{1/2})$exp and $(t_{1/2})_{\rm WU}$ are the experimental and theoretical half-life values, of which the latter is obtained from a Weisskopf estimate. The degree of forbiddeness, ν, is defined for a transition of multipole order λ as $\nu = \Delta K - \lambda$. This f_ν factor is usually of the order of 100 [33] but may vary substantially. This is especially true for $E1$ transitions, which are typically delayed even without any K hindrance [33]. For example, the observed $\Delta K = 5$ $E1$ transitions for transuranium elements ^{236,240}Pu [34] and ^{254}No [14], range from $f_\nu = 340$ to 835. Our values $f_\nu(296\ \text{keV}) = 596$, $f_\nu(447\ \text{keV}) = 538$, and $f_\nu(586\ \text{keV}) = 937$ are in that range. Large f_ν values for transitions depopulating the high-K isomeric state suggest stiff axial deformation and a low amount of Coriolis mixing in the $11/2^-$ rotational band in ^{257}Rf [35].

C. Model calculations of multiquasiparticle configurations

Additional support for the proposed decay scheme comes from configuration-constrained potential-energy-surface calculations [36] in deformation space (β_2, β_4, β_6) performed as part of this work. The higher-order deformation β_6 has been found to be important for the description of multi-QP states in nuclei around ^{254}No [37]. The triaxiality parameter γ has been assumed to be negligible for the well-deformed prolate nuclei in the region. In these calculations, the single-particle orbitals are obtained from the axially deformed Woods-Saxon potential with the set of universal parameters [38]. The pairing correlations are treated by means of the Lipkin-Nogami method [39] with the strength determined by the average gap method [40]. The unpaired nucleon orbits that specify a given configuration are blocked at each point of the deformation lattice, which is achieved by calculating and identifying the

TABLE VI. Calculated 1-QP and 3-QP configurations for ^{257}Rf.

Configuration	K^π	$E_x^{calc.}$
$\nu 1/2^+[620]$	$1/2^+$	0
$\nu 11/2^-[725]$	$11/2^-$	104
$\pi^2(1/2^-[521] \otimes 9/2^+[624])_{5^-} \otimes \nu 11/2^-[725]$	$21/2^+$	1150
$\pi^2(7/2^-[514] \otimes 9/2^+[624])_{8^-} \otimes \nu 11/2^-[725]$	$27/2^+$	1227
$\nu^2(9/2^-[734] \otimes 1/2^+[620])_{5^-} \otimes \nu 11/2^-[725]$	$21/2^+$	1393
$\nu^2(9/2^-[734] \otimes 7/2^+[613])_{8^-} \otimes \nu 11/2^-[725]$	$27/2^+$	1427
$\pi^2(1/2^-[521] \otimes 5/2^-[512])_{3^+} \otimes \nu 11/2^-[725]$	$17/2^+$	1439
$\nu^2(9/2^-[734] \otimes 3/2^+[622])_{6^-} \otimes \nu 11/2^-[725]$	$23/2^+$	1484
$\pi^2(7/2^+[514] \otimes 5/2^-[512])_{6^+} \otimes \nu 11/2^-[725]$	$23/2^-$	1531
$\pi^2(7/2^+[514] \otimes 1/2^+[521])_{4^+} \otimes \nu 11/2^-[725]$	$19/2^-$	1538

average Nilsson quantum numbers for every orbit involved in the configuration. The total energy of a state consists of a macroscopic part that is obtained with the standard liquid-drop model [41] and a microscopic part that is calculated by the Strutinsky shell-correction approach, including blocking effects. The calculated properties of single-QP and multi-QP levels in ^{257}Rf and ^{256}Rf are presented in Tables VI and VII, respectively.

There are two candidates for the proposed $(21/2^+)$ assignment, formed by coupling of the $11/2^-[725]$ single-quasineutron state to either the $(1/2^-[521] \otimes 9/2^+[624])_{5^-}$ two-quasiproton or the $(9/2^-[734] \otimes 1/2^+[620])_{5^-}$ two-quasineutron configuration. The quasiproton excitation is favored since it is located lower in energy and agrees with the experimental energy within 100 keV. Its decay to the rotational band based on the $11/2^-$-state is in agreement with assumptions of the decay path of lowest possible ΔK and involves no change of the unpaired neutron in the initial and final states.

The observation of the $1/2^-[521]$ proton state is of particular interest, since it originates from the $2f_{5/2}$ spherical shell located above the $Z = 114$ shell gap. It has strongly downsloping behavior and intrudes among the prolate-deformed configurations originating from the $2f_{7/2}$, $1i_{13/2}$, and $1h_{9/2}$ spherical shells. Therefore, its location and evolution is important for the predictions of the magnitude of the possible $Z = 114$ spherical shell gap. It has been observed at low excitation energies in ^{251}Md ($Z = 99$) [42] and ^{253,255}Lr ($Z = 101$) [43–45]. In addition, the $(1/2^-[521] \otimes 7/2^-[514])_{3^+}$ two-quasiproton configuration has been suggested for the lowest two-QP excitation in ^{254}No [14,46], which fits with similar observation here.

TABLE VII. Calculated 2-QP configurations for ^{256}Rf.

Configuration	K^π	$E_x^{calc.}$
$\pi^2(1/2^-[521] \otimes 9/2^+[624])$	5^-	1062
$\pi^2(7/2^-[514] \otimes 9/2^+[624])$	8^-	1102
$\pi^2(7/2^-[514] \otimes 5/2^-[512])$	3^+	1346
$\nu^2(9/2^-[734] \otimes 1/2^+[620])$	5^-	1350
$\nu^2(9/2^-[734] \otimes 7/2^+[613])$	8^-	1390
$\pi^2(7/2^+[514] \otimes 5/2^-[512])$	6^+	1411
$\pi^2(7/2^+[514] \otimes 1/2^+[521])$	4^+	1425
$\nu^2(9/2^-[734] \otimes 3/2^+[622])$	6^-	1446
$\nu^2(9/2^-[734] \otimes 11/2^-[725])$	10^+	1455
$\pi^2(9/2^+[624] \otimes 5/2^-[512])$	7^-	1507

In general, the calculated energies of the two-quasiproton excitations are lower compared to the two-quasineutron excitations (see Table VII). This is consistent with the observation of the deformed neutron shell gap at $N = 152$ [8,13]. To form a two-quasineutron state, the unpaired neutron is required be excited across the gap, which is reflected in higher excitation energies. On the other hand, a recent experimental work [31] suggests no significant deformed shell gap at $Z = 104$, in agreement with low energies for the proton excitations; see Sec. IV D.

D. Re-interpretation of the isomers in ^{256}Rf

The suggested 3-QP configuration for the second isomer in ^{257}Rf allows us to re-interpret the isomeric states in ^{256}Rf. Three multi-QP isomeric states having similar half-lives (around 20 μs) have been observed [12]. Of these isomers the lowest one was suggested to have $K = 6$ or 7 and the second-lowest $K = 10$–12. The latter isomer, located at ≈1400 keV, was interpreted to have the $\nu^2(9/2^-[734] \otimes 11/2^-[725])_{10^+}$ configuration and the lower-lying one, located at ≈1120 keV, was suggested to have a nonspecified two-quasineutron configuration. The third isomer, located above 2 MeV, was suggested as having a 4-QP configuration. The proposed 3-QP configuration $\pi^2(1/2^-[521] \otimes 9/2^+[624])_{5^-} \otimes \nu 11/2^-[725]$ for ^{257}Rf^{m2} suggests that the $K^\pi = 5^-$ analoguous two-quasiproton configuration is responsible for the lowest isomeric state in ^{256}Rf. This is supported by the calculations presented in Table VII. This $K^\pi = 5^-$ state may then decay into a rotational band based on the 2^- intermediate state as suggested in Ref. [12]. Similar 2^- states have been observed for several $N = 150$ isotones and they are generally interpreted as having octupole vibrational character, although they are often dominated by a single quasiparticle component in the wave function.

The second isomer in ^{256}Rf may decay into a rotational band based on the first isomeric state. One can estimate the energies of that band based on the rotational model (1), which yields $E(7^-) \approx 1270$, $E(8^-) \approx 1360$, and $E(9^-) \approx 1470$ keV, respectively, by using $\hbar^2/2J = 5.8$ typical for 2-QP bands in ^{250}Cf. The energy of the second isomer (≈1400 keV [12]) is between the estimated energies of the 8^- and 9^- states favoring a spin of 8^- instead of previously suggested 10^+. The calculations predict two $I^\pi = 8^-$ states above 1 MeV. Of those states the $(7/2^-[514] \otimes 9/2^+[624])_{8^-}$ two-quasiproton configuration located lower in energy may be favored, since the possible decay to the lower-lying isomer requires only a $1/2^-[521] \rightarrow 7/2^-[514]$ proton transition. A possible decay scenario of the two lower isomeric states in ^{256}Rf is presented in Fig. 10.

In this scenario, both isomers decay by $\Delta K = 3$, $M1$ transitions having transition energies of tens of kilo electron volts, corresponding to hindrance factors on the order of a few thousands. This scenario offers an explanation for the similar half-lives of both states. Although this interpretation is

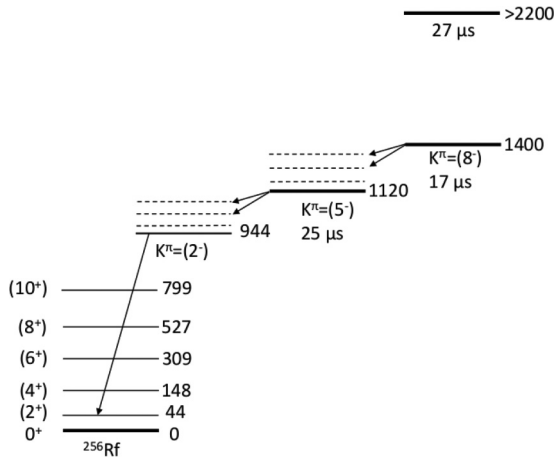

FIG. 10. Possible decay scheme for ^{256}Rf, adopted from Ref. [12]. The spin assignments for isomeric states are from this work.

very speculative, it agrees with the experimental isomeric-state energies, as well as the observation of only one strong 900-keV multipolarity-$E1$ transition, interpreted to occur between the lowest 2^- and 2^+ states. The other transitions would be of low energy, highly converted, and therefore would not be observed experimentally. Other scenarios, such as transitions populating states with $I^\pi > 4^+$ in the ground-state band, would yield observable effects, as discussed in Ref. [12].

There has been a recent experimental study of the K isomers in ^{256}Rf by Rubert *et al.* [47], which largely confirms the experimental findings of Ref. [12]. It will be interesting to see if the data can shed more light on the nature of the high-K isomers in ^{256}Rf. Most likely, further experimental work will be required to firmly pin down spin-parity and configuration assignments. For example, the gyromagnetic ratios of the rotational bands based on the isomeric states would be among the key observables in future studies.

V. CONCLUSIONS

To conclude, ^{257}Rf has been studied via delayed γ-ray and electron decay spectroscopy. The high-K isomeric state in ^{257}Rf has been observed to decay to a rotational band based on the $11/2^-[725]$ neutron excitation. Based on its decay properties, a spin of $(21/2^+)$ has been proposed, which may correspond to the $\pi^2(1/2^-[521] \otimes 9/2^+[624])_{5^-} \otimes \nu 11/2^-[725]$ three-quasiparticle configuration. This interpretation implies the analogous two-quasiproton configuration for the lowest isomeric state in ^{256}Rf. The suggested configurations favor low-energy two-quasiproton states, suggesting that the $N = 152$ gap persists for the $Z = 104$ Rf nuclei.

ACKNOWLEDGMENTS

We are grateful to Jerome Rubert and Benoit Gall of IPHC Strasbourg for sharing with us their results on ^{256}Rf prior to publication and for many illuminating discussions. We thank the 88-Inch Cyclotron operations staff for providing the beams for this experiment. This work was supported in part by the U.S. Department of Energy under Contract No. DE-AC02-05CH11231 (LBNL) and No. DE-AC52-07NA27344 (LLNL), and the Swedish Research Council (LU). U.F. acknowledges support from the Royal Physiographic Society in Lund.

[1] N. Bohr and J. A. Wheeler, Phys. Rev. **56**, 426 (1939).
[2] S. Ćwiok *et al.*, Nucl. Phys. A **611**, 211 (1996).
[3] A.T. Kruppa, M. Bender, W. Nazarewicz, P. G. Reinhard, T. Vertse, and S. Cwiok, Phys. Rev. C **61**, 034313 (2000).
[4] M. Bender, K. Rutz, P.-G. Reinhard, J. A. Maruhn, and W. Greiner, Phys. Rev. C **60**, 034304 (1999).
[5] R.-D. Herzberg *et al.*, Nature (London) **442**, 896 (2006).
[6] S. K. Tandel *et al.*, Phys. Rev. Lett. **97**, 082502 (2006).
[7] B. Sulignano *et al.*, Eur. Phys. J. A **33**, 327 (2007).
[8] P. T. Greenlees *et al.*, Phys. Rev. C **78**, 021303 (2008).
[9] K. Hauschild *et al.*, Phys. Rev. C **78**, 021302 (2008).
[10] A. P. Robinson *et al.*, Phys. Rev. C **78**, 034308 (2008).
[11] H. B. Jeppesen *et al.*, Phys. Rev. C **80**, 034324 (2009).
[12] H. B. Jeppesen *et al.*, Phys. Rev. C **79**, 031303 (2009).
[13] J. Qian *et al.*, Phys. Rev. C **79**, 064319 (2009).
[14] R. M. Clark *et al.*, Phys. Lett. B **690**, 19 (2010).
[15] F. P. Hessberger *et al.*, Eur. Phys. J. A **43**, 55 (2010).
[16] J. S. Berryman *et al.*, Phys. Rev. C **81**, 064325 (2010).
[17] A. Lopez-Martens *et al.*, Nucl. Phys. A **852**, 15 (2011).
[18] S. Antalic *et al.*, Eur. Phys. J. **47**, 62 (2011).
[19] B. Sulignano *et al.*, Phys. Rev. C **86**, 044318 (2012).
[20] F. P. Hessberger *et al.*, Z. Phys. A **359**, 415 (1997).
[21] B. Streicher *et al.*, Eur. Phys. J. A **45**, 275 (2010).
[22] C. M. Folden, Ph.D. thesis, University of Berkeley, 2004.
[23] I. Dragojević *et al.*, Phys. Rev. C **78**, 024605 (2008).
[24] J. F. Ziegler, computer software SRIM, http://www.srim.org/.
[25] G. Dûchene *et al.*, Nucl. Instrum. Methods Phys. Res., Sect. A **432**, 90 (1999).
[26] G. Jones, Nucl. Instrum. Methods Phys. Res., Sect. A **488**, 471 (2002).
[27] J. A. Becker *et al.*, Phys. Rev. C **41**, R9 (1990).
[28] C. S. Wu, J. Y. Zeng, Z. Xing, X. Q. Chen, and J. Meng, Phys. Rev. C **45**, 261 (1992).
[29] P. Walker *et al.*, Nucl. Phys. A **568**, 397 (1994).
[30] L. Esser, U. Neuneyer, R. F. Casten, and P. von Brentano, Phys. Rev. C **55**, 206 (1997).
[31] P. T. Greenlees *et al.*, Phys. Rev. Lett. **109**, 012501 (2012).
[32] R. R. Chasman, I. Ahmad, A. M. Friedman, and J. R. Erskine, Rev. Mod. Phys. **49**, 833 (1977).
[33] K. Löbner, Phys. Lett. B **26**, 369 (1968).
[34] M. Asai *et al.*, Eur. Phys. J. A **23**, 395 (2005).
[35] P. M. Walker, J. Phys. G. **16**, L233 (1990).
[36] F. R. Xu, P. M. Walker, J. A. Sheikh, and R. Wyss, Phys. Lett. B **435**, 257 (1998).
[37] H. L. Liu, F. R. Xu, P. M. Walker, and C. A. Bertulani, Phys. Rev. C **83**, 011303 (2011).
[38] W. Nazarewicz, J. Dudek, R. Bengtsson, T. Bengtsson, and I. Ragnarsson, Nucl. Phys. A **435**, 397 (1985).

[39] H. C. Pradhan, Y. Nogami, and J. Law, Nucl. Phys. A **201**, 357 (1973).
[40] P. Möller and J. R. Nix, Nucl. Phys. A **536**, 20 (1992).
[41] W. D. Myers and W. J. Swiatecki, Nucl. Phys. **81**, 1 (1966).
[42] A. Chatillon *et al.*, Phys. Rev. Lett. **98**, 132503 (2007).
[43] F. Hessberger *et al.*, Eur. Phys. J. A **12**, 57 (2001).
[44] A. Chatillon *et al.*, Eur. Phys. J. A **30**, 397 (2006).
[45] S. Ketelhut *et al.*, Phys. Rev. Lett. **102**, 212501 (2009).
[46] S. Eeckhaudt *et al.*, Eur. Phys. J. A **26**, 227 (2005).
[47] J. Rubert, Ph.D. thesis, University of Strasbourg, 2013.